Submitted, accepted and published by:
Chemical Engineering Science 62 (2007) 533 – 549

Mapping of the Range of Operational Conditions for Cu-, Fe-, and Ni-based Oxygen Carriers in Chemical-Looping Combustion

Alberto Abad, Juan Adánez [1], Francisco García-Labiano, Luis F. de Diego, Pilar Gayán, Javier Celaya

Instituto de Carboquímica (C.S.I.C), Department of Energy and Environment, Miguel Luesma Castán 4, Zaragoza 50015, Spain

Abstract

Chemical-Looping Combustion (CLC) is a two-step combustion process that produces a pure CO_2 stream, ready for compression and sequestration. A CLC system is composed by two reactors, an air and a fuel reactor, and an oxygen carrier circulating between the reactors, which transfers the oxygen necessary for the fuel combustion from the air to the fuel. This system can be designed similar to a circulating fluidized bed, but with the addition of a bubbling fluidized bed on the return side. A mapping of the range of operational conditions, design values, and oxygen carrier characteristics is presented for the most usual metal oxides (CuO, Fe_2O_3, and NiO) and different fuel gases (CH_4, H_2, and CO). The pressure operation of a CLC system is also considered. Moreover, a comparison of the possible use of three high reactive oxygen carriers (Cu10Al-I, Fe45Al-FG, Ni40Al-FG) previously characterised is carried out. It was found that the circulation rates and the solids inventories are linked, and the possible operating conditions are closely dependent on the reactivity of the oxygen carriers. The operational limits of the solids circulation rates, given by the mass and heat balances in the system, were defined for the different type of oxygen carriers. Moreover, a plot to calculate the solids inventories in a CLC system, valid for any type of oxygen carrier and fuel gas, is proposed. The minimum solids inventories depended on the fuel gas used, and followed the order CH_4>CO>H_2. Values of minimum solids inventories in a range from 40 to 170 kg/MW_f were found for the oxygen carriers used in this work. From the economic analysis carried out it was found the cost of the oxygen carrier particles does not represent any limitation to the development of the CLC technology.

[1] Corresponding author: Tel.: +34-976-733977; fax: +34-976-733318. *E-mail address:* jadanez@icb.csic.es (Juan Adánez)

Keywords: Design; Environment; Fluidization; Kinetics; Chemical-Looping Combustion; Oxygen Carriers

1. Introduction

The problem of global warming caused by the greenhouse gas emissions is nowadays gaining increasing importance. Commercially available CO_2 capture technologies are high cost and their use today will significantly increase the cost of electricity and heat generation. This fact has produced an important development of CO_2 capture technologies to reduce the energy needs for separation and thereby, the costs per tonne of CO_2 avoided. Three main routes can be explored to limit CO_2 emissions: post-combustion capture, precombustion decarbonisation, and denitrogenated conversion. For each one of these routes a wide array of technologies is being presently evaluated from a technical and economical point of view.

In this sense, Chemical-Looping Combustion (CLC) has been revealed as an efficient and low costly process. This new type of combustion, initially proposed by Ritcher and Knoche (1983), leads to beneficial exergy efficiencies in the system if CO_2 capture is considered (Wolf et al., 2005). Wolf et al. (2001) reported a thermal efficiency as high as 52-53% in a combined cycle CLC plant operating at 1200 ºC in the air reactor and 13 bars, which represents a 5 percent more efficient process than a natural gas with combined cycle system with state-of-the-art technology for CO_2 capture. The efficiency would be something lower in an atmospheric CLC operating in a steam cycle. However, different economic assessments performed by the CCP (CO_2 Capture Project) (Kerr, 2005) and by the International Panel on Climate Change (IPCC, 2005) indicated CLC among the best options for reducing the cost of CO_2 capture using fuel gas.

CLC is a two-step gas combustion process that produces a pure CO_2 stream, ready for compression and sequestration. A solid oxygen carrier (OC) circulates between two reactors and transports oxygen from the combustion air to the fuel. Since the fuel is not mixed with air, the subsequent CO_2 separation process is not necessary. As gaseous fuel can be used natural gas or synthesis gas from coal gasification. In this system, the total amount of heat evolved from reactions in the two reactors is the same as for normal combustion, where the oxygen is in direct contact with fuel.

Since the process requires a good contact between gas and solids as well as a flow of solid material between the fuel and air reactors, the use of two interconnected fluidized beds have advantages over other designs (see Figure 1). The bed material circulating between the two

fluidized beds is the oxygen carrier in the form of metal oxide particles. The volumetric gas flow in the air reactor is approximately 2.5 and 10 times larger than that of syngas and CH_4, respectively, because a large amount of nitrogen in the air is carried out. To keep a reasonable size of the reactors a high velocity riser was proposed for the air reactor (Lyngfelt et al., 2001) in a CLC plant using CH_4 as fuel gas. In the air reactor (AR), oxygen is transferred from the combustion air to the oxygen carrier. The exit gas stream from the air reactor contains N_2 and some unused O_2. The particles carried away from the riser are recovered by a cyclone and led to the fuel reactor (FR). In the fuel reactor (bubbling fluidized bed) oxygen is transferred from the oxygen carrier to the fuel. The exit gas stream from the fuel reactor contains CO_2 and H_2O, and almost pure CO_2 is obtained after H_2O condensation. From the fuel reactor the particles are returned to the air reactor by gravity. Two particle seals prevent gas mixing between the two reactors. The technical risk of the system is therefore relatively low operating at atmospheric pressure because all the processes are carried out in standard process equipment and using elements of proven technology (Copeland, 2001; Lyngfelt et al., 2001).

Ideally, the number of reduction-oxidation cycles of the oxygen carrier would be infinite. However, the oxygen carrier material must be renovated as a consequence of particle attrition/fragmentation or reactivity loss during the reduction/oxidation cycles and a makeup flow of new material (F_0) is necessary. Since the cost of this new material is the main additional cost of the whole process compared to a process without CO_2 capture, the key issue in the system performance is the oxygen carrier material. Besides high reactivity toward the fuel gas and air during many reduction-oxidation cycles, the oxygen carriers must fulfil other characteristics as high resistance to attrition, no presence of agglomeration, and no carbon deposition when using carbon-included fuels. Other environmental and economical aspects must be also considered in the final selection of the oxygen carrier.

There are in the literature several works related with design of CLC reactors. Lyngfelt et al. (2001) presented the first design of an atmospheric CLC reactor including a high-velocity riser for the air reactor and a low-velocity fluidized bed for the fuel reactor. A conceptual design of a 10 kW thermal power CLC working at atmospheric pressure was done by Kronberger et al. (2005a). Wolf et al. (2005) analyzed the feasibility of CLC in two interconnected pressurized fluidized bed reactors for a capacity of 800 MW input of natural gas.

Other authors have analysed specific aspects of the CLC process. Adánez et al. (2003) presented a model for the optimization of the fuel reactor operation. Johansson et al. (2003) analysed the gas leakage between the reactors, and Kronberger et al. (2004) used a cold model to find critical design parameters of the CLC system.

The CLC process has been successfully demonstrated in a 10 kW unit (Lyngfelt et al., 2004; Lyngfelt and Thunman, 2005) during 100 h of continuous operation burning natural gas and using a Ni-based oxygen carrier. Moreover, Ryu et al. (2004) presented the results of 3.5 hour continuous run in a 50 kW Chemical-Looping Combustor. The following steps in the process development will include a design optimization, continuous operation during long time at pilot plant scale, and detailed engineering and cost analysis at higher scales. Moreover, the chemical and mechanical stability of the oxygen carriers must be proved during long time.

The objective of this work is to determine the relation between suitable operating conditions in a CLC process and oxygen carrier characteristics for different Cu-, Fe-, and Ni-based materials and fuel gases (CH_4, H_2, and CO). Moreover, a comparison of the behavior in a CLC process of three oxygen carriers previously characterised is showed.

2. Oxygen Carriers

Different metal oxides have been proposed in the literature (Ritcher and Knoche, 1983; Ishida et al., 1987; Mattisson and Lyngfelt, 2001) as possible candidates for CLC process: CuO, NiO, Mn_2O_3, Fe_2O_3, and CoO. In general, these metal oxides are combined with an inert which acts as a porous support providing a higher surface area for reaction, as a binder for increasing the mechanical strength and attrition resistance, and, additionally, as an ion conductor enhancing the ion permeability in the solid.

Among them, iron, nickel, and copper have been selected as the most promising candidates to be used in a CLC process (Adánez et al., 2004). Oxides of these metals supported on several inerts showed low attrition rates and high reaction rates during many successive reduction-oxidation cycles (Mattisson et al., 2003; Kronberger et al., 2004; Adánez et al., 2004, 2005) although their behavior during continuous operation must be proved.

Table 1 shows the reduction reactions of these metal oxides with CH_4, H_2, and CO, and the oxidation reactions with O_2. An important characteristic of the metal oxides is their oxygen transport capacity, also called oxygen ratio (Mattisson et al., 2003), defined as $R_o=(m_{ox}-m_{red})/m_{ox}$, where m_{ox} and m_{red} are the masses of the oxidised and reduced form of the metal oxide, respectively. The oxygen transport capacity is the mass fraction of oxygen that can be used in the oxygen transfer. The maximum values correspond to the NiO and CuO and this is lower for the Fe_2O_3 in its transformation to Fe_3O_4. Although iron compounds have different oxidation states (Fe_2O_3-Fe_3O_4-FeO-Fe), only the transformation from hematite to magnetite may be applicable for industrial CLC systems. Further reduction to FeO would produce a high decrease in the CO_2 purity

obtained in the fuel reactor because of the increase of the CO and H_2 concentrations in the equilibrium (Copeland et al., 2001; Kronberger et al., 2005b). Obviously, the transport capacity of the oxygen carriers decreases due to the presence of the inert. In this way, the oxygen transport capacity of the oxygen carriers depends both on the active metal oxide content and on the type of metal oxide considered, $R_{o,OC}=R_o\ x_{MeO}$.

In this work, three oxygen carriers using Al_2O_3 as support have been considered: particles of copper (II) oxide prepared by impregnation (Aldrich Chemical Company), and iron- and nickel-based particles prepared by freeze-granulation at Chalmers University of Technology. The samples were designated as Cu10Al-I, Fe45Al-FG, and Ni40Al-FG. In all cases, part of the metal oxide used in the preparation reacts with the support to give aluminates that, in the majority of the cases, was not active for reaction. Table 2 shows the main properties of the materials.

For a better comparison of the effect of the type of metal oxides on their behavior in a CLC process, oxygen carriers with the same metal oxide content would be desirable. However, the Cu-based oxygen carriers with high CuO content undergo agglomerattion problems during their operation in a fluidized bed (de Diego et al., 2005). Therefore, the oxygen carrier Cu10Al-I presents a much lower MeO content than the other oxygen carriers.

2.1. Reactivity of the oxygen carriers

The reactivity of the oxygen carriers is an important factor to be considered in the design of a CLC process, because it is directly related with the solids inventory in the system. The oxygen carrier must have enough reactivity to fully convert the fuel gas in the fuel reactor, and to be regenerated in the air reactor.

The kinetics of the reduction and oxidation reactions of the three oxygen carriers based on Cu. Fe, and Ni were determined at atmospheric pressure in a thermobalance (CI Electronics Ltd.) at different operating conditions. More details about the experimental systems and operating procedures can be found elsewhere (García-Labiano et al., 2004). The temperature range was varied from 600 ºC to 950 ºC for the Fe45Al-FG and Ni40Al-FG oxygen carriers and from 500 ºC to 800 ºC for the Cu10Al-FG. The composition of the gas used to determine the kinetic of the reduction reaction was varied to cover the great majority of the gas concentrations present in the fluidized bed fuel reactor of a CLC system including the product gases (Fuel: 5-70 vol %; H_2O: 0-48 vol %; CO_2: 0-40 vol %). For the oxidation reaction, oxygen concentrations from 5 to 21 vol % were used.

As an example, Figure 2 shows the conversion versus time curves for the reduction and oxidation of the three oxygen carriers using a gas concentration of 15 vol %, corresponding

aproximately to the average concentration existing in a bubbling fluidized bed for the typical CLC reactions (see eq. 19). The three oxygen carriers were very reactive, although the reactivity of the Cu10Al-I oxygen carrier was higher than the reactivity of the others, Fe45Al-FG and Ni40Al-FG. However, this difference in reactivity can not be directly translated into solids inventory data for the CLC process, as a consequence of their different oxygen transport capacity (see Table 2).

There are several resistances that can affect the reaction rate of the oxygen carrier with the fuel gas or with the air. Previous calculations showed that the mass transfer resistances in the gas film and in the product layer of the particle were not important in the experimental conditions used in this work. To determine the kinetic parameters of these oxygen carriers with respect to the reduction (CH_4, H_2, and CO) and oxidation reactions (O_2) the shrinking core model (SCM) with the reaction controlled by the chemical reaction in the grain was used. Two different geometries were considered taking into account the structural differences of the oxygen carriers. Fe- and Ni-based oxygen carriers prepared by freeze-granulation exhibited a granular structure, and the SCM for spherical grains was considered. However, the SCM for plate-like geometry in the porous surface of the particle was considered for the Cu-based oxygen carrier prepared by impregnation assuming a uniform layer of metal oxide inside the pores covering the inert material. The equations that describe these models under chemical reaction control in the grain are the following:

for spherical grain geometry

$$\frac{t}{\tau} = 1-(1-X_s)^{1/3} \qquad \tau = \frac{\rho_m\, r_g}{b_i\, k\, (C^n - C_{eq}^n)} \tag{1}$$

for plate-like geometry

$$\frac{t}{\tau} = X_s \qquad \tau = \frac{\rho_m\, L}{b_i\, k\, C^n} \tag{2}$$

where the kinetic constant follows an Arrhenius type dependence with temperature

$$k = k_0\, e^{-E/RT} \tag{3}$$

Eq. (1) considers the thermodynamic equilibrium for the reactant gas that occurs in the Ni-based oxygen carriers, especially when working with H_2 or CO. For the other metal oxides the value of C_{eq} is zero. Table 3 shows the values of the kinetic parameters obtained at atmospheric pressure for the different oxygen carriers and reactions used in this work (García-Labiano et al., 2005; Adánez, 2005). The activation energies determined were low, with values ranging from 7 to 78 kJ/mol, and are similar to those reported in literature (Ishida et al., 1996; Ryu et al., 2001). The reaction order depended on the reacting gas, and values from 0.2 to 1 were found. The gas products (CO_2 and

H_2O) did not affect the reduction reaction rates. Only during the reduction of the Fe45Al-FG oxygen carrier with CH_4 a negative effect of the H_2O on the direct reaction rate was observed. In this case, the total reaction time was calculated as

$$\tau_{r,CH_4} = \frac{\rho_m \, r_g}{b_{CH_4} \, k \, (1 - 0.15 C_{H_2O}) \, C_{CH_4}^{0.3}} \tag{4}$$

The effect of total pressure on the reaction rate of the oxygen carriers Cu10Al-I, Fe45Al-FG, and Ni40Al-FG with H_2, CO, and O_2 was analysed in a previous work (García-Labiano et al., 2005). The experiments showed that an increase in total pressure had a negative effect on the reaction rate of all oxygen carriers and reactions. An apparent preexponential factor was determined as a function of total pressure and the preexponential factor obtained at atmospheric pressure to fit the experimenatl data

$$k_{0,p} = \frac{k_0}{P^q} \tag{5}$$

The values of the parameter "q" for each oxygen carrier and reaction are showed in Table 3.

3. Design criteria for a CLC system

According to Lyngfelt et al. (2001), the three main parameters for the design of a CLC system are: 1) the amount of bed material in the two reactors, that must be adequate for a sufficient conversion of reacting gas, 2) the circulation rate between the reactors, that must be high enough to transfer the oxygen necessary for the fuel combustion and the heat necessary to maintain the heat balance, and 3) the gas leakage between the reactors must be minimised.

The two first are dependent on characteristics of the oxygen carrier used, as solid reactivity, type of metal oxide, and weight content. This section analyses the main differences existing in the use of Cu-, Fe-, and Ni-based oxygen carriers in relation with the design of a CLC system. Moreover, the possibility of use of the three oxygen carriers previously characterised (Cu10Al-I, Fe45Al-FG, Ni40Al-FG) is included.

3.1. Mass Balance. The CLC concept is based on the transport of oxygen from the air to the fuel by means of an oxygen carrier. Fig. 1 shows the general scheme of a CLC system. Ideally, the oxygen carrier should circulate in the system an infinite number of cycles. However, a makeup flow of new solids, F_0, is required to compensate for the natural decay of activity and/or solid losses by attrition/fragmentation during operation.

The mass balance in the system, based on molar flow of oxygen carrier fully oxisided, is as follows,

FR $$\left(F_R - F_1\right)\Delta X_{s,FR} + F_0\,\Delta X_{s,F_0} = b_r\,F_f\,\Delta X_f \tag{6}$$

AR $$F_R\,\Delta X_{s,AR} = c_o\,F_{O_2}\Delta X_{O_2} \tag{7}$$

where $\Delta X_{s,F0}$ is the conversion variation of the fresh particles fed into the system due to the reaction with the gas in the fuel reactor. For steady state operation, $F_1=F_0$, and if the oxygen carrier is valid for the use in CLC, the condition $F_0<<F_R$ is required to keep the sorbent makeup cost within reasonable limits, and it can be assumed with low error that

$$F_{O_2}\Delta X_{O_2} = \frac{b_r}{c_o}\,F_f\Delta X_f = d\,F_f\Delta X_f \tag{8}$$

and

$$\Delta X_{s,AR} = \Delta X_{s,FR} \tag{9}$$

where the parameter "d" is the stoichiometric factor in the fuel combustion reaction.

3.2. Circulation rate. The circulation rate, expressed as mass flow of oxygen carrier totally oxidised, depends on the type of oxygen carrier and fuel used, as well as on the conversion variation obtained in the oxygen carrier in the fuel and air reactors, and it can be obtained from Eq. (6)

$$\overset{\circ}{m}_{OC} = 10^{-3}\,\frac{b_r\,M_{MeO}\,F_f\,\Delta X_f}{x_{MeO}\,\Delta X_{s,FR}} \tag{10}$$

Taking as reference 1 MW of fuel, and assuming full conversion of gas (ΔX_f=1), Eq. (10) can be rewritten as

$$\dot{m}_{OC} = \frac{b_r\,M_{MeO}}{x_{MeO}\,\Delta H_c^0}\,\frac{1}{\Delta X_{s,FR}} = \frac{\dot{m}_c}{\Delta X_{s,FR}} \tag{11}$$

where the characteristic circulation rate, $\dot{m}_c$, is a specific parameter defined by the oxygen carrier-fuel pair.

$$\dot{m}_c = \frac{b_r\,M_{MeO}}{x_{MeO}\,\Delta H_c^0} = \frac{2\,d\,M_O}{R_{o,OC}\,\Delta H_c^0} \tag{12}$$

Although Eq. (11) gives the circulation rate necessary to fulfill the oxygen mass balance in the CLC system, it is also necessary to consider other aspects related with the hydrodynamic behavior and with the heat balance in the system.

The circulation rate in a CFB system depends on the operation conditions and configuration of the riser. There are several works that have mapped possible combinations of fluidisation velocities, riser pressure drop and external solids flux (Takeutchi et al, 1986; Lim et al., 1995). For typical conditions of gas velocity (4-6 m/s), temperature (850-950 ºC), and excess of air (0-20%), values of riser areas in a CLC process from 0.12 to 0.35 m^2/MW_f are obtained considering the combustion of CH_4, H_2, or CO (0.18-0.35 for CH_4, 0.12-0.25 for CO, 0.15-0.29 for H_2). Selecting a value of 0.2 m^2/MW_f as an average value of the cross section area of the riser, S, the solids flow can be calculated as:

$$G_s = \frac{\dot{m}_{OC}}{S} \tag{13}$$

Fig. 3 shows the circulation rates, G_s, for the different metal oxides (CuO, Fe_2O_3, and NiO) and fuel gas considered in this work as a function of the metal oxide content in the oxygen carrier and on its conversion variation. Obviously, the values of G_s decrease with increasing the MeO content of the oxygen carrier.

The Fe-based oxygen carriers need much higher circulation rates than the Ni- and Cu-based oxygen carriers, because of their low oxygen transport capacity (see Table 1). The differences in G_s as a consequence of the fuel gas used are of lower importance. The solid flow is linked with the oxygen needed for the reaction of each fuel gas. Thus, to obtain 1 MW are necessary 1.25 mol CH_4 s^{-1}, 3.53 mol CO s^{-1}, or 4.14 mol H_2 s^{-1} as a consequence of their different combustion heat (see Table 1), and the transport of 5, 4.14, or 3.53 mol O s^{-1}, respectively.

The limit of the circulation rate in a CLC plant is not clear. When the gas velocity in a circulating fluidized bed is increased the circulation flow increases up to point where the recycling system is not dimensioned to accomodate a larger flow. Larger flows can be reached by redesigning of the recycling system. However, very large flows could generate increased difficulties with entraining gas between reactors and increasing costs if they are outside the range of normal commercial experience. Although there is some dispersion in the experimental data available in the literature, values of G_s from 20 to 100 kg m^{-2} s^{-1} have been reported for CFB systems (Smolders and Baeyens, 2001). Lyngfelt et al. (2001) yield values of G_s in the order of 50 kg m^{-2} s^{-1} for the combustion of natural gas using iron oxide as oxygen carrier in a CLC plant under atmospheric conditions. Taking 80 kg m^{-2} s^{-1} as the maximum circulation rate feasible in a CLC plant without increased costs and with commercial experience, it can be observed that it would be impossible to work with Fe-based oxygen carriers with Fe_2O_3 contents lower than 10 wt. % because the circulation rate would prevent the full conversion of gas even with infinite solids inventory

(ΔX_s=1). The higher transport capacity of the other metal oxides (CuO, NiO) makes possible the preparation of oxygen carriers with low MeO contents. In these cases, values about 10-20 wt% could be enough for normal operation without high circulation rates.

Other important aspect to be considered in a CLC system is the heat balance. The oxidation reaction of the metal oxides is always exothermic. The reduction reaction can be endothermic or exothermic depending on the metal oxide and fuel gas combination, although the great majority of the heat, even for exothermic reductions, is generated in the air reactor (see Table 1).

For endothermic reduction reactions (NiO with CH_4, Fe_2O_3 with CH_4), the fuel reactor is heated by the circulating solids coming from the air reactor at higher temperature. As previously have been seen (Fig. 3), the solid circulation rates depend on the MeO content and on its conversion variation, ΔX_s. Therefore, for a fixed temperature in the air reactor, the temperature in the fuel reactor will depend on the same variables. Fig. 4 shows the effect of the MeO content and the ΔX_s values on the temperature in FR for the combustion of CH_4 with a Ni-based oxygen carrier for a fixed temperature in AR of 950 ºC. The heat extracted from the AR is necessary to fulfill the heat balance in the system, considered as an adiabatic system. When the solids circulation rate decreases, which corresponds to higher MeO content or higher ΔX_s (see Fig. 3), the temperature in FR also decreases because less heat is transfered from the AR. To avoid a large temperature drop in the FR, a high solids circulation rate is desired, which in practice means a low ΔX_s. In a real situation, the energy losses in the system will make necessary even higher circulation rates than the above showed, and so lower ΔX_s. Similar results are obtained when a Fe-based oxygen carrier is used for the combustion of CH_4. However, the temperature drop in FR is lower in this case because the Fe-based oxygen carriers need a higher circulation rate to fulfill the mass balance as a consequence of their low oxygen transport capacity (see Table 1). In all these situations, it would be necessary to limit the temperature drop in the FR to maintain a high reduction reaction rate and to get full gas conversion.

Fig. 5 shows the MeO content necessary to maintain a temperature difference of 50 ºC between the air and fuel reactors for the reduction reactions of Fe- and Ni-based oxygen carriers with CH_4 as a function of ΔX_s. It can be observed that Ni-based oxygen carriers with low NiO contents or low ΔX_s values must be used in the system; however, Fe-based oxygen carriers with high Fe_2O_3 contents and high ΔX_s can be used to maintain a temperature difference lower than 50 ºC. It can be concluded that when the reduction reaction is endothermic, the circulation rate is limited between the maximum given by the riser capacity and the minimum given by the heat balance (see Fig. 3).

When the reduction reaction is exothermic (see Table 1), the solids circulation rate is not limited by the heat balance. In this case, the circulation rate will be selected to reach the desired solid conversion in the air reactor. Fig. 5 shows the combinations between MeO content and circulation rate, expressed as ΔX_s, that produces an increase of temperature of 50 ºC in FR. It is observed that, for Cu-based oxygen carriers, this temperature increase is reached at low values of CuO content or low ΔX_s. Similar situations can be reached for the combustion of syngas with Ni- or Fe-based oxygen carriers, although in this case the difference of temperature is reached at high MeO contents and high ΔX_s. For the reaction of Fe_2O_3 with syngas, a gradient of temperature of 50 ºC was not obtained in any case, even considering a MeO content of 100 wt % and a ΔX_s=1.

3.3 Solids inventories

In a CLC process, it is desirable to minimise the amount of bed material in the reactors because this will reduce the size and investment cost of the system and also less power will be needed by the fans that supply the reacting gases to the reactors, especially to the air reactor.

The solids inventory in the CLC system for any fuel conversion can be obtained from a mass balance of the solid and gas in the fuel and air reactors. For preliminary estimations, it has been considered that the reactions between the gas fuel and air with the oxygen carrier take place in bubbling fluidized beds. Although the air reactor must be normally a riser, it is very probable that the higher residence time of the solids, and then the oxidation reaction, take place in the dense zone at the bottom of the riser. Therefore, in this work, the fuel and air reactor are treated in a similar way. For preliminary calculations, it was assumed perfect mixing of the solids, gas plug flow in the beds, and no resistance to the gas exchange between the bubble and emulsion phases.

For the complete conversion of the gas, the mass of oxygen carrier in each reactor per MW of fuel, expressed as mass of oxygen carrier totally oxidised, can be calculated as shown in García-Labiano et al. (2004)

$$m_{OC,FR} = \dot{m}_c \frac{\tau_r}{\Phi_{FR}} \tag{14}$$

$$m_{OC,AR} = \dot{m}_c \frac{\tau_o}{\Phi_{AR}} \tag{15}$$

where the characteristic reactivity, Φ_{FR} or Φ_{AR}, are parameters defined as

$$\Phi_{FR} = \left[\tau_r \overline{\frac{dX_s}{dt}} \right]_{FR} \tag{16}$$

$$\Phi_{AR} = \left[\tau_o \overline{\frac{dX_s}{dt}} \right]_{AR} \tag{17}$$

The total solids inventory in the system, per MW of fuel, will be given by

$$m_{OC,AR+FR} = m_{OC,AR} + m_{OC,FR} \tag{18}$$

The characteristic circulation rate $\dot{m}_c$ was defined by Eq. (12), and the specific values for the oxygen carriers Cu10AL-I, Fe45Al-FG, and Ni40Al-FG are showed in Table 3. For the calculation of the solids inventory in the air reactor, the value of $\dot{m}_c$ corresponding to the fuel used in the system must be considered.

The values of τ_r and τ_o for the reduction and oxidation reactions were obtained at an average gas concentration. Assuming perfect mixing of solids, gas plug flow in the reactors and no resistance to the gas exchange between bubble and emulsion phases in the fluidized bed, the average concentration of reacting gas in their respective reactors can be obtained from the following equation (see Appendix II):

$$\overline{C^n} = \frac{\Delta X_g C_0^n}{\int_{X_{g,in}}^{X_{g,out}} \left[\frac{1+\varepsilon_g X_g}{1-X_g} \right]^n dX_g} \tag{19}$$

The parameter ε_g in Eq. (19) considers the gas expansion as a consequence of the reaction, and it was calculated as

$$\varepsilon_g = \frac{V_{g,X_g=1} - V_{g,X_g=0}}{V_{g,X_g=0}} \tag{20}$$

The value of ε_g was 2 for the reduction reaction with CH_4, 0 for the use of H_2 and CO, and -0.21 for the oxidation reaction. Table 3 shows the average concentration considering full conversion of gas in the fuel reactor, and an air excess of 20 % in the air reactor.

Assuming perfect mixing of the solids in the reactors, the characteristic reactivity, Φ_j, can be expressed in each reactor (FR or AR) as a function of the solid conversion at the inlet and the conversion variation in the reactor (see Appendix I),

for spherical grain geometry

$$\Phi_j = 3\left[1 - X_{o,inj}^{2/3}\exp\left(-\frac{\left(1 - X_{o,inj}^{1/3}\right)}{\Delta X_s}\Phi_j\right)\right] - \frac{6\Delta X_s}{\Phi_j}\left[1 - X_{o,inj}^{1/3}\exp\left(-\frac{\left(1 - X_{o,inj}^{1/3}\right)}{\Delta X_s}\Phi_j\right)\right] + \frac{6\Delta X_s^2}{\Phi_j^2}\left[1 - \exp\left(-\frac{\left(1 - \overline{X}_{o,inj}^{1/3}\right)}{\Delta X_s}\Phi_j\right)\right] \quad (21)$$

for plate-like geometry

$$\Phi_j = 1 - \exp\left(-\frac{\left(1 - X_{o,inj}\right)}{\Delta X_s}\Phi_j\right) \quad (22)$$

The characteristic reactivity, Φ_j, is very useful to calculate the solids inventory because this is only a function of the solid conversion at the inlet and the conversion variation reached in each reactor, and it is valid for any solid reactivity and oxygen transport capacity. An important fact is that the value of this term is limited between 0 and 3 for the use of the SCM with spherical grains, and between 0 and 1 for plate-like geometry.

Therefore, the solids inventory for a given oxygen carrier and fuel gas depends on the solids circulation rate and on the solid conversion at the inlet to each reactor, as well as on their metal oxide content and reactivity. Fig. 6 shows the total solids inventory, $m_{OC,AR+FR}$, of oxygen carrier Ni40Al-FG per MW_f of CH_4 in the CLC system as a function of the oxidation conversion at the outlet of the air reactor, $\overline{X}_{o,out\,AR}$, and the variation of solid conversion between the two reactors, ΔX_s. Obviously, $\overline{X}_{o,out\,AR} = \overline{X}_{o,in\,FR}$. The level curves indicate the conditions with a same amount of oxygen carrier in the CLC system. From this diagram it is possible to know the total solids inventory for a given solid recirculation as a function of the average solid conversion from the air reactor $\overline{X}_{o,out\,AR}$. It can be observed that, for a given ΔX_s, the total solid inventory presents a minimum with $\overline{X}_{o,out\,AR}$ due to the effect of the average conversion on the characteristic reactivity of each reactor, Φ_{AR} and Φ_{FR}, and therefore in the solids inventory. On the other hand, for a given $\overline{X}_{o,out\,AR}$, the solid inventory in the whole CLC system increases as ΔX_s increases. The minimum solids inventory in the system is reached at ΔX_s near to zero, in this case, 32 kg per MW_f.

Similar diagrams can be obtained for the different oxygen carriers and fuel gases. However, this type of graphs is only valid for each specific oxygen carrier and fuel gas, and can be very different depending on the reactivity of the material. To generalise this study, Fig. 7 shows a new design plot valid for any oxygen carrier and fuel gas reacting under shrinking core model with chemical

reaction control for spherical grains. The optimum solid inventory in a CLC system can be obtained from the use of this plot and Eqs. (14) to (18). The inlet variables are the type of oxygen carrier ($R_{o,OC}$) and the fuel gas, which define the value of $\dot{m}_c$, the reactivity of the oxygen carrier during reduction and oxidation, defined by the τ_i values, and the circulation rate.

Fig. 7 shows the value of Φ_j as function of the solid conversion at the inlet of the fuel reactor, $\overline{X}_{o,in\,FR}$, or in the air reactor, $\overline{X}_{o,in\,AR}$, and ΔX_s for the SCM with spherical grains. For a given pair of values ($\overline{X}_{o,in\,FR}$, ΔX_s) it is possible to know the value of Φ_{FR} from the plot. Similarly, for the air reactor, the value of Φ_{AR} is obtained from the pair of values ($\overline{X}_{o,in\,AR}$, ΔX_s). The solids inventory in each reactor can be calculated then from Eqs. (14) and (15) and the total solids inventory in the system by Eq. (18). Fig. 7 also shows the relation between the circulation rate, expressed as $\dot{m}_{OC}/\dot{m}_c$ and ΔX_s given by Eq. (11). It can be observed that a decrease in the circulation rate produces a decrease in the value of the Φ_j parameter, both for the fuel and air reactors. Therefore, the solids inventory increase when the circulation rate decreases. For a fixed circulation rate of a given oxygen carrier, there is only a value of ΔX_s that fulfil the mass balance in the system. As previously shown, at this condition the total solids inventory has a minimum value as a function of $\overline{X}_{o,out\,AR}$ (see Fig. 6). This minimum inventory depends on the values of τ_r and τ_o, defined by the gas-solid reactivity. Fig. 7 shows different curves to obtain the minimum solids inventory for several values of τ_r/τ_o or τ_o/τ_r. The crossing point of ΔX_s and τ_r/τ_o line determines the Φ_{FR} value for the total minimum inventory at a fixed ΔX_s, and the corresponding value of solid conversion at the inlet of FR. The solids inventory in FR can be directly calculated from Eq. (14). On the other hand, the crossing point of ΔX_s and τ_o/τ_r line determines the Φ_{AR} value and the solids inventory in AR can be calculated from Eq. (15). The value of the solid conversion at the inlet of AR that gives the minimum solids inventory in the system can be obtained directly from the above crossing point.

As example, for a ΔX_s=0.3 and an oxygen carrier with values of τ_r=30 s and τ_o= 6 s, the conditions for the minimum solids inventory in FR are reached at the point (ΔX_s=0.3, τ_r/τ_o=5), which gives values of Φ_{FR}=2.2 and $\overline{X}_{o,in\,FR}$=0.75. For AR, the point (ΔX_s=0.3, τ_o/τ_r=0.2) give values of Φ_{AR}=2 and $\overline{X}_{o,in\,AR}$ =0.45. Obviously, $\overline{X}_{o,in\,FR} = \overline{X}_{o,in\,AR} + \Delta X_s$. The solids inventories in FR and AR can be calculated directly from Eqs. (14) and (15).

The optimum operating conditions in the CLC system are those that give the minimum solids inventory at a fixed ΔX_s and get full gas conversion. These conditions will be considered from now on. Fig. 8 shows the minimum solids inventory and the circulation rate necessary for the full

conversion of CH_4 as a function of ΔX_s for the three oxygen carriers selected in this work. Similar curves can be obtained for the fuel gases H_2 or CO although the differences in the values can be high, up to a decrease of 30% in G_s and a decrease of 70% in the the minimum solids inventory. Low values of ΔX_s gave high circulation rates and low solids inventory. Oppositely, high values of ΔX_s gave low circulation rates, but high solids inventory. Assuming a maximum circulation rate in the system of 80 kg m^{-2} s^{-1}, the ΔX_s values must be higher than 0.04, 0.28, and 0.34 for the oxygen carriers Ni40Al-FG, Cu10Al-I, and Fe45Al-FG, respectively. The optimum values of ΔX_s to get low circulation rates and low solids inventory could be about 0.2-0.4, because higher values of ΔX_s highly increase the solid inventories. Table 4 shows the minimum solids inventory in the fuel and air reactors per MW_f of CH_4, H_2 and CO for ΔX_s close to zero and ΔX_s=0.3. Although the oxidation rate is the same independently of the gas used for the reduction, the differences observed among gas fuels in the air reactor inventory are due to the different oxygen flows necessary to fulfill the mass balance in the system.

It is observed that the use of the oxygen carrier Fe45Al-FG for the combustion of CH_4 in a CLC process needs the higher solids inventory, because although it is a very reactive solid, its low oxygen transport capacity produces low reaction rates per kg of oxygen carrier. The Ni40Al-FG oxygen carrier needs lower solids inventory because its high reaction rate and high oxygen transport capacity. On the other hand, the values for the Cu10AL-I oxygen carrier was between the above given for the other oxygen carriers, as a consequence of their low CuO content but high oxygen transport capacity of the CuO. Similar curves can be obtained for the other fuel gases (H_2, CO). All these values correspond to conditions where the resistance to the gas exchange between the bubble and emulsion phases has been considered negligible. In real systems, if the resistance to the gas exchange between the bubble and emulsion phases is important, the τ_i values would increase and as a consequence, higher solids inventories and so, higher residence time of the solids in the reactors would be predicted.

Estimations of the total inventory in a CLC system with different oxygen carriers and CH_4 as fuel gas can be found in the literature. Mattisson et al. (2003) estimated that the amount of oxygen carrier was 70 kg per MW in the fuel reactor, and 390 kg per MW in the air reactor, using a 33 wt % CuO oxygen carrier prepared by dry impregnation. Cho et al. (2004) obtained that the bed mass in the fuel reactor was 200 kg per MW with a 60 wt % CuO oxygen carrier produced by freeze granulation. However, for their calculus, they did not consider the solids residence time distribution and use the reactivity obtained at a determined solid conversion. The data showed by these authors were higher than those obtained in the present work because of the lower reactivity of their materials.

3.4. Relation between oxygen transport capacity, solid reactivity and solids inventory

As above showed in Eqs. (14) and (15), the solids inventory in each reactor depends on the solids reactivity through the parameter τ_r or τ_o, on the oxygen transport capacity of the oxygen carrier, $R_{o,OC}$, through the parameter $\dot{m}_c$, and on ΔX_s through the parameter Φ_j (see Fig. 7). Therefore, for a given circulation rate, that is for a given ΔX_s, there are pair of values $R_{0,carrier}$-τ_i that generates the same solids inventory. Fig. 9 shows the solids inventories, in FR or AR, obtained for the CH_4 combustion. These values were obtained for $\Delta X_s < 0.05$ which correspond to minimum values of solids inventory in the system.

It can be observed that a same inventory can be reached with an oxygen carrier with less oxygen transport capacity but with higher reactivity. Fig. 9 also shows the points corresponding to the oxygen carriers used in this work (Cu10Al-I, Fe45Al-FG, and Ni40Al-FG). For example, the reactivity of the Fe45Al-FG oxygen carrier with CH_4 (τ_r=53 s) is higher than the reactivity of the Ni40Al-FG (τ_r =60 s). However, this increase is not enough to compensate their lower oxygen transport capacity, and higher solids inventories are necessary ($m_{Fe45Al\text{-}FG}$ =100 kg/MW_{CH4}, $m_{Ni40Al\text{-}FG}$ =19 kg/MW_{CH4}). Fig. 9 also shows the circulation rates, expressed as $G_s \Delta X_s$, as a function of the $R_{o,OC}$. Metal oxides with low oxygen transport capacity, as for example the Fe_2O_3, needs high metal oxide contents, normally above 40%, to fulfil the mass balance in the system.

3.5. Effect of total pressure in CLC systems

The use of a pressurized CLC system would have several advantages with respect to the atmospheric operation. First, the efficiency of the cycle in the CLC power plant will be increased (Wolf et al., 2001); second, the recovering of the CO_2 as a high-pressure gas requires only a very small amount of additional power for further compressing the CO_2 to pipeline (35 atm) or sequestration pressure (100 atm) (Copeland et al., 2001).

The total pressure can affect to important operating and design parameters of the CLC system. A higher pressure produces an increase in the gas molar concentration, thus an increase in the reaction rate of the oxygen carriers would be expected. This will produce a large decrease in the solids inventory of the CLC system as well as in the size of the fluidized bed reactors. However, the experimental work carried out with the oxygen carriers Cu10Al-I, Fe45Al-FG, and Ni40Al-FG at total pressures up to 30 bars showed that, oppositely to the expected, an increase in operating pressure did not produced the expected increase in the reaction rates (García-Labiano et al., 2005).

Table 4 shows the values predicted for the different oxygen carriers at 10 bars, considering that according to Wolf et al. (2001) the pressure has no significant impact on the efficiency of the plant at a range from 10 to 18 bars. For the same gas linear velocity, the increase of the operating pressure produces a decrease in the cross section area of the reactors. Therefore, the higher value of the ratio between solids inventories and cross section area will translate into taller beds for pressure CLC systems in comparison to the atmospheric operation.

Other important fact will be related with the solids circulation rates. It must be considered that the circulation flow needs to be larger per cross section area at increasing pressure when compared to atmospheric operation. In this case, the values of G_s showed in Fig. 3 should be multiplied by the operating pressure, which would have important consequences on the CLC operation as well as in the selection of the oxygen carrier. For example, the use of Fe-based oxygen carriers at a total pressure of 10 bars is difficult, or the MeO content of the Cu- and Ni-based oxygen carriers must be increased up to values above 60% in order to use lower values of ΔX_s, and consequently as lower solid inventories as possible.

3.6. Economic analysis and performance of the oxygen carrier

There are nowadays a wide range of technologies for the CO_2 capture and storage (CCS), which have different maturity levels. Since any kind of power plants have yet built at a full scale with CCS, the costs of these systems cannot be stated with a high degree of confidence at this time Therefore, it is beyond the scope of this section to do an exhaustive economic analysis of the CLC in comparison with other CCS processes as done by IPCC (IPCC, 2005). The aim is only to establish a link between the expected cost of an oxygen carrier and its expected performance in a CLC system.

The main advantage of the CLC process compared to normal combustion is that CO_2 is not diluted with N_2 in the combustion gases and almost pure CO_2 is obtained without any extra energy needed. Therefore, the cost of fresh oxygen carrier cost added to the system is potentially the biggest cost per ton of CO_2 avoided in a CLC process. There was even a concern that the cost of the particles could be a show-stopper for this technology (Lyngfelt and Thunman, 2005). The oxygen carrier cost is related with the makeup flow, because of the natural decay of activity and/or losses during many reduction-oxidation cycles. Thus, the cost of the makeup flow of oxygen carrier per tonne of CO_2 avoided, χ_{OC}, can be defined by

$$\chi_{OC} = 10^3 \, \dot{\mu}_{0,OC} \, C_{OC} \qquad (23)$$

where C_{OC} is the unit cost of solid oxygen carrier ($/kg OC) and $\dot{\mu}_{0,OC}$ the flow of new oxygen carrier added (kg/s) per kg/s of CO_2 avoided. Fig. 10 shows the value of χ_{OC} as a function of the makeup flow, $\dot{\mu}_{0,OC}$, for several costs of the oxygen carrier, C_{OC}. A decrease of this cost allows a decrease of the CO_2 capture costs and/or an increase of the makeup flow to maintain constant the χ_{OC} value.

The cost of the oxygen carrier, C_{OC}, will be the sum of several factors including the cost of the metal oxide, the inert, and the manufacture cost,

$$C_{OC} = x_{MeO} C_{MeO} + (1 - x_{MeO}) C_I + C_m \quad (24)$$

The costs of the metal, C_{MeO}, for the oxygen carriers considered in this work were 0.03 $/kg Fe_2O_3, 2.9 $/kg Cu and 13.8 $/kg Ni (US Geological Survey, 2005) considered to be the raw material, and the cost of the inert, C_I, was 0.5 $/kg Al_2O_3. According to Lyngfelt and Thunman (2005) the manufacture costs of the oxygen carriers were about 1$/kg OC. These costs are low, although the cost in the process will depend on the lifetime of the particles.

To have a general idea of the lifetime of the particles in the reactors, it has been considered as reference value the cost of CO_2 capture for a proven process as it is the absorption with methanolamine, MEA. In these systems, the cost of CO_2 capture is about 60 $/tonne CO_2 avoided (Rao and Rubin, 2002). The most of this cost, 47 $/tonne CO_2 avoided, is associated with the CO_2 capture process, and from this cost only 6 $/tonne CO_2 proceed from the makeup flow of MEA, because this process has an important energy penalty.

From Eq. (24) or Fig. 10(a) can be obtained the make-up flow of fresh oxygen carrier, per kg/s of CO_2 avoided, that gives a χ_{OC} values of 6$ per ton CO_2 avoided. These values, per ton of CO_2 avoided, were $3.6 \cdot 10^{-3}$ kg/s, $4.9 \cdot 10^{-3}$ kg/s, and $7.8 \cdot 10^{-4}$ kg/s for the oxygen carriers Cu10Al-I, Fe45Al-FG, and Ni40Al-FG, respectively.

On the other hand, the make-up flow of fresh oxygen carrier together with the total solids inventory define the residence time, or lifetime (LT), of the oxygen carriers in the CLC system,

$$LT = \frac{\mu_{OC,AR+FR}}{\dot{\mu}_{0,OC}} \quad (25)$$

where $\mu_{OC,AR+FR}$ is the solids inventory per kg/s of CO_2 avoided

$$\mu_{OC,AR+FR} = \frac{\Delta H_c^0}{s_e M_{CO_2}} m_{OC,AR+FR} \quad (26)$$

The lifetime of the oxygen carriers was defined as the mean time that a particle of oxygen carrier must be under reaction, reduction or oxidation, in the system without any reactivity loss or without suffer the attrition/fragmentation processes that produce the particles elutriation out of the system. $m_{OC,AR+FR}$ can be calculated with Eqs. (14) to (18) and Fig. 7. The specific emission, s_e, is defined as the moles of CO_2 produced per mol of fuel gas. For example, s_e is 1 for CH_4 and 0.67 for a synthesis gas composed by 67 vol % CO and 33 vol % H_2.

Fig. 10(b) shows the lifetime of the oxygen carriers as a function of the makeup flow for several solids inventories, $\mu_{OC,AR+FR}$. Fig. 10 also shows the lines corresponding to the oxygen carriers used in this work for the combustion of CH_4, and for a ΔX_s value of 0.3. Considering a cost of oxygen carrier, χ_{OC} of 6 \$/tonne of CO_2 avoided, it was obtained a lifetime about 180 h for the Cu10Al-I and Fe45Al-Fg oxygen carriers, and about 290 h for the Ni40Al-FG. These data are not very high, and are even lower if we consider as reference the target range of \$20-30 per tonne of CO_2 avoided proposed for future CO_2 capture processes (Kerr, 2005). In this case, the lifetime required for the particles would be under 100 h, which have been yet reached in a 10-kW CLC prototype located at Chalmers University (Lyngfelt and Thunman, 2005). Therefore, the problem of use particles with low lifetime arrives from the cost derived of the safe disposal of the residues generated in the process as well as from the stronger filtration system required in the plant, especially if CLC is used in a gas turbine cycle.

The unit cost of oxygen carrier, C_{OC}, could be different to that assumed above. The consideration of the additional cost due to the safe disposal of the material used can increase the cost of the oxygen carriers in the process. On the other hand, if the material lost in the process can be used as raw material in the production of new oxygen carrier, the cost will decrease. In any case, the new lifetime of the oxygen carrier can be recalculated as

$$LT_2 = \frac{C_{OC,2}}{C_{OC,1}} LT_1 \quad (27)$$

Eq. (26) and Fig. 10 show that the necessary lifetime of the particles in the system increases with an increase of the solids inventory, $\mu_{OC,AR+FR}$. Therefore, those design variables affecting the solids inventories as the oxygen carrier reactivity or circulation rates will also affect the lifetime values. That is, an increase of the oxygen carrier reactivity or on the circulation rate will reduce the solids inventory in the whole CLC system, and so the cost of the CO_2 capture.

On the other hand, the consideration of other aspects affecting the gas-solid reaction in the fluidized bed as the resistance to the gas exchange between bubble and emulsion phases, or the bad solids mixing in the fluidized bed will produce an increase in the solids inventory and in the costs of the CO_2 capture. Moreover, a possible loss of reactivity of the oxygen carrier during cyclic reactions, or the chemical poisoning of the active part of the material, increases the solids inventory needed in the system, and decreases the lifetime allowable in the system. Both factors gives an increase in the makup flow of the oxygen carrier, $\dot{\mu}_{0,OC}$, and therefore in the cost, χ_{OC}.

Lyngfelt and Thunman (2005) reported the operational experience of the 10-kW CLC prototype using Ni-based particles during 100 h of combustion conditions, and 300 h considering also the time that the particles have been circulating at high temperature. No decrease in reactivity was detected during the test period and from their elutriation results a lifetime of the particles of 40000 h was inferred. This value is very much higher to the about obtained for different reference costs. Even assuming a lifetime of the particles one order of magnitude lower, 4000 h, the cost of the particles will be about 0.3-0.4 \$/tonne CO_2. From the analysis carried out, it can be concluded that the cost of the particles does not represent a limitation to the technology development, and make of the CLC a very promising process for CO_2 capture if oxygen carriers with enough reactivity and high attrition resistance are produced. This agree with the economic assessments performed by the CCP (CO_2 Capture Project) and by the IPCC (IPCC, 2005) which indicated CLC among the best options for reducing the cost of CO_2 capture using fuel gas (Kerr, 2005).

Conclusions

The design and operation conditions of a CLC system highly depend on the type of oxygen carrier used. This work shows the range of suitable operating conditions with respect to solids circulation rates, and calculates the solids inventories needed to operate a CLC process for the different Cu-, Fe-, and Ni- based oxygen carriers and different fuel gases (CH_4, H_2, and CO). It was found that both design parameters are linked and depend on the reactivity and oxygen transport capacity of the oxygen carrier.

The circulation rates were defined for the different type of oxygen carriers and fuel gases as a function of the metal oxide content. The differences in the solids flux, G_s, as a consequence of the fuel gas used were of low importance. When the reaction in the fuel reactor was endothermic, a minimum circulation rate was necessary to avoid a strong decrease in the fuel reactor temperature.

The Fe-based oxygen carriers need much higher circulation rates than the Ni- and Cu-based oxygen carriers, because of their low oxygen transport capacity. Assuming a maximum feasible circulation rate in the CLC system of 80 kg m^{-2} s^{-1} the use of these oxygen carriers with MeO contents below 10 wt% is prevented, because the oxygen transferred could be lower than oxygen needed. On the other hand, the higher transport capacity of the other metal oxides (CuO, NiO) make possible the preparation of oxygen carriers with lower MeO contents, and values about 10-20 wt% could be enough for normal operation.

The solids inventory for a given oxygen carrier and fuel gas depends on the solids circulation rate and on the oxygen carrier characteristics, as their metal oxide content and reactivity with respect to the reduction and oxidation reactions. In this sense, a plot to calculate the solids inventories in a CLC system, valid for any oxygen carrier and fuel gas, is proposed. For a typical CLC operation, the minimum solids inventories per MW_f depended on the fuel gas used, and followed the order CH_4>CO>H_2. Values of minimum solids inventories, for ΔX_s=0.3, in a range from 40 to 170 kg/MW_f were found. Moreover, the relation between oxygen transport capacity, solids reactivity and solids inventory was defined. It was found that a same inventory can be obtained with an oxygen carrier with less oxygen transport capacity but with higher reactivity.

Some design parameters of a pressurised CLC system based on kinetic data previously obtained were also explored. It was found that the operation of a pressurised CLC system will need higher solids inventories that the expected by an increase in the gas concentration at higher pressures. The pressure operation also affects to the circulation rates. It was found that the operation with any Fe-based oxygen carrier at a total pressure of 10 bars could be quite difficult, because the upper limit for the transport capacity of solids in the riser. On the other hand, the MeO content of the Cu- and Ni-based oxygen carriers must be increased up to values above 60%.

From the economic analysis carried out it was found the cost of the particles does not represent any limitation to the development of the CLC technology. Considering the makeup flow of the particles as the main cost associated to the process, a lifetime of the particles of about 300 h represents the same cost of material that the makeup of amine in a proven technology of CO_2 capture as it is the absorption with MEA. In addition, particles with lifetime under 100 h would fulfill the target range of 20-30$ per tone of CO_2 avoided proposed for future CO_2 capture processes. However, the cost of the safe disposal of the residues generated in this case and the filtration system required in the plant would be limitant aspects to be consider in the CLC development when using particles with low lifetime.

Acknowledgements

This work was carried out with financial support from the European Coal and Steel Community (Project 7220-PR/125), and the Spanish Ministry of Education and Science (Project CTQ2004-04034).

Nomenclature

b_i = stoichiometric factor for the reaction i, mol solid reactant (mol fuel)$^{-1}$
c_o = stoichiometric factor in the oxidation reaction, mol solid product (mol O_2)$^{-1}$
C = gas concentration, mol m^{-3}
C_0 = gas concentration at X_g=0, mol m^{-3}
C_{eq} = gas concentration at equilibrium conditions, mol m^{-3}
$\overline{C}$ = average gas concentration, mol m^{-3}
C_{OC} = unit cost of sorbent or oxygen carrier, \$ (kg OC)$^{-1}$
C_{MeO}= unit cost of the active metal in the oxygen carrier, \$ (kg MeO)$^{-1}$
C_I= unit cost of the inert in the oxygen carrier, \$ (kg inert)$^{-1}$
C_m= manufacture cost of the oxygen carrier, \$ (kg OC)$^{-1}$
d= stochiometric factor in the fuel combustion reaction with oxygen, mol O_2 per mol of fuel
E = activation energy, J mol^{-1}
F_0 = molar makeup flow of MeO, (mol MeO) s^{-1}
F_l= molar flow of MeO elutriated from the system, (mol MeO) s^{-1}
F_f = molar flow of fuel gas, (mol fuel) s^{-1}
F_{O2} = molar flow of O_2 in the air reactor, (mol O_2) s^{-1}
F_R = molar circulation flow of MeO between the air and fuel reactors, (mol MeO) s^{-1}
G_s = specific solids circulation rate per MW_f, kg m^{-2} s^{-1} MW_f^{-1}
k = chemical reaction rate constant, mol^{1-n} m^{3n-2} s^{-1}
k_0= preexponential factor of the chemical reaction rate constant, mol^{1-n} m^{3n-2} s^{-1}
$k_{0,P}$= preexponential factor of the chemical reaction rate constant at pressure P, mol^{1-n} m^{3n-2} s^{-1}
L = layer thickness of the reacting solid, m
LT= lifetime of the oxygen carrier, s
$m_{OC,j}$= total solid inventory, as fully oxidized oxygen carrier, in the reactor j, (kg OC) MW_f^{-1}
$m_{OC,AR+FR}$ = total solid inventory, as fully oxidized oxygen carrier, (kg OC) MW_f^{-1}
$\overset{\circ}{m}_{OC}$ = circulation rate of fully oxidized oxygen carrier, (kg OC) s^{-1}
$\dot{m}_{OC}$ = circulation rate of fully oxidized oxygen carrier, (kg OC) s^{-1} MW_f^{-1}
$\dot{m}_c$ = characteristic circulation rate defined in Eq. (12), (kg OC) s^{-1} MW_f^{-1}
M_{CO2} = molecular weight of the carbon dioxide, 44 g mol^{-1}
M_{MeO} = molecular weight of the metal oxide, g mol^{-1}
M_O = molecular weight of oxygen, 16 g mol^{-1}
m_{ox}= mass of the oxidised form of the metal oxide, g
m_{red}=mass of the reduced form fo the metal oxide, g
n = reaction order
P = total pressure, atm
q = exponent of P in Eq. (5)
r_g = grain radius, m
R = constant of the ideal gases, J mol^{-1} K^{-1}
R_o = oxygen transport capacity of the metal oxide
$R_{o,OC}$ = oxygen transport capacity of the oxygen carrier
S = cross section area of the riser per MW_f, m^2 MW_f^{-1}
s_e= specific emission, moles CO_2 (mol of fuel gas)$^{-1}$
t = time, s
T = temperature, K
$V_{g,Xg=0}$ = volume of the gas mixture at X_g=0, m^3
$V_{g,Xg=1}$ = volume of the gas mixture at X_g=1, m^3

x_{MeO} = mass fraction of MeO in the fully oxidized sample
X_g = gas conversion
$X_{g,in}$ = gas conversion at the reactor inlet
$X_{g,out}$ = gas conversion at the reactor outlet
X_s = solid conversion
$\overline{X}_{o,inj}$ = average solid conversion at the inlet of the reactor j
$\overline{X}_{o,outj}$ = average solid conversion at the outlet of the reactor j

Greek letters
χ_{OC} = cost of makeup flow of oxygen carrier per tonne of CO_2 avoided, \$ (ton CO_2)$^{-1}$
ΔH_c^0 = standard heat of combustion of the gas fuel, kJ mol^{-1}
ΔT = variation of the solids temperature between the inlet and outlet temperatures in the fuel reactor, K
ΔX_f = variation of the fuel conversion
ΔX_g = variation of the gas conversion
$\Delta X_{s,j}$ = variation of the solid conversion in the reactor j
$\Delta X_{s,F0}$ = variation of the conversion of the fresh particles fed into the system due to the reaction with the gas in the fuel reactor
ε_g = coefficient of expansion of the gas mixture
Φ_j=characteristic reactivity inthe reactor j defined in Eqs. (16) and (17)
$\mu_{OC,AR+FR}$ = total solid inventory, as fully oxidized oxygen carrier, defined per kg/s of CO_2, kg MeO (kg CO_2/s)$^{-1}$
$\dot{\mu}_{0,OC}$ =makeup flow of oxygen carrier added per kg/s of CO_2 revomed, (kg OC) (kg CO_2)$^{-1}$
ρ_m = molar density of the reacting material, mol m^{-3}
τ_i = time for complete solid conversion for the reaction i, s

Subscripts
i = solid reaction (o: oxidation; r: reduction)
j = reactor (AR: air reactor; FR: fuel reactor)
g = reacting gas (CH_4, CO, H_2, O_2)
f = reacting fuel (CH_4, CO, H_2)

Appendix I. Characteristic reactivity.

The average reactivity of reacting solid in the fuel or air reactor can be calculated with the following equation, assuming the residence time distribution in the fuel or air reactor corresponding with a perfect mixing of solids in the reactors

$$\left[\overline{\frac{dX_s}{dt}}\right]_j = \int_0^{t_{c,j}} \left[\frac{dX_s}{dt}\right]_i \frac{e^{-t/t_{m,j}}}{t_{m,j}} dt \tag{A1}$$

where $t_{m,j}$ is the mean residence time of the oxygen carrier particles in the fuel or air reactor, which are dependent on the solid recirculation rate and on the reactor size

$$t_{m,j} = \frac{m_{ox}}{\dot{m}_{ox}} = \frac{\Delta X_s}{\left[\overline{\frac{dX_s}{dt}}\right]_j} \tag{A2}$$

The average reactivity have been expressed to consider that the oxygen carrier is introduced into the fuel and air reactors with a mean solid conversion, $\overline{X}_{r,inFR}$ or $\overline{X}_{o,inAR}$, higher than 0. Following a SCM under chemical reaction control, it was assumed that the unconverted solid was in the inner core of the grain or plate. The reacting time in the reactor j necessary to reach complete conversion will be $t_{c,j}$, being this value the upper limit of the integration in Eq. (A1), and was defined for the spherical grain geometry

$$t_{c,j} = \tau_i \left(1 - \overline{X}_{i,inj}^{1/3}\right) \tag{A3}$$

or for the plate-like geometry

$$t_{c,j} = \tau_i \left(1 - \overline{X}_{i,inj}\right) \tag{A4}$$

Integration of Eq. (A1) gives, for the SCM for spherical grains

$$\left[\overline{\frac{dX_s}{dt}}\right]_j = \frac{3}{\tau_i}\left[1 - \left(1 - \frac{t_{c,j}}{\tau_i}\right)^2 e^{-t_{c,j}/t_{m,j}}\right] - \frac{6t_{m,j}}{\tau_i^2}\left[1 - \left(1 - \frac{t_{c,j}}{\tau_i}\right) e^{-t_{c,j}/t_{m,j}}\right] + \frac{6t_{m,j}^2}{\tau_i^3}\left[1 - e^{-t_{c,j}/t_{m,j}}\right] \tag{A5}$$

and for the plate-like geometry

$$\left[\overline{\frac{dX_s}{dt}}\right]_j = \frac{1}{\tau_i}\left[1 - e^{-t_{c,j}/t_{m,j}}\right] \tag{A6}$$

From Eqs. (A2)-(A6) it can be obtained:

Spherical grains

$$\left[\overline{\frac{dX_s}{dt}}\right]_j = \frac{3}{\tau_i}\left[1 - \overline{X}_{i,inj}^{2/3}\exp\left(-\frac{\tau_j\left(1-\overline{X}_{i,inj}^{1/3}\right)}{\Delta X_s}\left[\overline{\frac{dX_s}{dt}}\right]_j\right)\right] -$$
$$-\frac{6\Delta X_s}{\tau_i^2\left[\overline{\frac{dX_s}{dt}}\right]_j}\left[1 - \overline{X}_{i,inj}^{1/3}\exp\left(-\frac{\tau_j\left(1-\overline{X}_{i,inj}^{1/3}\right)}{\Delta X_s}\left[\overline{\frac{dX_s}{dt}}\right]_j\right)\right] + \frac{6\Delta X_s^2}{\tau_i^3\left[\overline{\frac{dX_s}{dt}}\right]_j^2}\left[1 - \exp\left(-\frac{\tau_i\left(1-\overline{X}_{i,inj}^{1/3}\right)}{\Delta X_s}\left[\overline{\frac{dX_s}{dt}}\right]_j\right)\right] \tag{A7}$$

Plate-like geometry

$$\left[\overline{\frac{dX_s}{dt}}\right]_j = \frac{1}{\tau_i}\left[1 - \exp\left(-\frac{\tau_i\left(1-\overline{X}_{i,inj}\right)}{\Delta X_s}\left[\overline{\frac{dX_s}{dt}}\right]_j\right)\right] \tag{A8}$$

Eqs. (21) and (22) were obtained multiplying Eq. (A7) and (A8) by τ_i.

Appendix II. Average concentration.

The values of τ_i, for the reduction or oxidation reactions, were obtained at an average gas concentration, $\overline{C}$. Assuming perfect mixing of solids and gas plug flow in the reactors and no resistance to the gas exchange between bubble and emulsion phases in the fluidized bed, the can be obtained for the design of the fuel reactor (Levenspiel, 1981)

Perfect mixing of solids:

$$\frac{V_{MeO}}{F_{MeO}} = \frac{\Delta X_s}{\left(-\bar{r}_{MeO}\right)_{PM}}, \qquad \text{being } \left(-\bar{r}_{MeO}\right)_{PM} = \rho_{m,MeO}\left[\overline{\frac{dX_s}{dt}}\right]_{\overline{C}} \tag{A9}$$

Gas plug flow:

$$\frac{V_{MeO}}{F_g} = \int_{X_{g,in}}^{X_{g,out}} \frac{dX_g}{\left(-\bar{r}_g\right)_{PF}}, \qquad \text{being } \left(-\bar{r}_g\right)_{PF} = \frac{\rho_{m,MeO}}{b_r}\left[\overline{\frac{dX_s}{dt}}\right] \tag{A10}$$

Similar equations can be obtained for the air reactor. From these equations it can be obtained that

$$m_{MeO} = \frac{\rho_{MeO}}{\rho_{m,MeO}} b_r F_g \frac{\Delta X_g}{\left[\overline{\frac{dX_s}{dt}}\right]_{\overline{C}}} \tag{A11}$$

$$m_{MeO} = \frac{\rho_{MeO}}{\rho_{m,MeO}} b_r F_g \int_{X_{g,e}}^{X_{g,s}} \frac{dX_g}{\left[\overline{\frac{dX_s}{dt}}\right]} \tag{A12}$$

The solids inventory obtained from Eq. (A11) must be the same that this obtained from Eq. (A12), and the following equation is obtained:

$$\frac{\Delta X_g}{\left[\overline{\frac{dX_s}{dt}}\right]_{\overline{C}}} = \int_{X_{g,e}}^{X_{g,s}} \frac{dX_g}{\left[\overline{\frac{dX_s}{dt}}\right]} \tag{A13}$$

The average concentration of reacting gas in their respective reactor, $\overline{C}$, is those that fulfill Eq. (A13) using the average reactivity shown in Eq. (A7) or (A8), and defined by Eq. (19).

Literature Cited

Adánez, J., García-Labiano, F., de Diego, L. F., Plata, A., Celaya, J., Gayán, P., Abad, A., 2003. Optimizing the fuel reactor for chemical-looping combustion. Proceedings of the 17th International Conference on Fluidized Bed Combustion. Jacksonville, USA. FBC2003-063.

Adánez, J., de Diego, L. F., García-Labiano, F., Gayán, P., Abad, A., Palacios, J. M., 2004. Selection of oxygen carriers for chemical-looping combustion. Energy Fuels, 18, 371-377.

Adánez, J. Capture of CO_2 in coal combustion. 2005. ECSC final report. Project No. 7220-PR125)

Adánez, J.; García-Labiano, F.; de Diego, L. F.; Gayán, P.; Abad, A.; Celaya, J., 2005. Development of oxygen carriers for chemical-looping combustion. In *Carbon Dioxide Capture for Storage in Deep Geologic Formations - Results form the CO_2 Capture Project*. Thomas, D., Benson, S. Eds. Volume 1, Chapter 34. Elsevier Ltd.,Oxford, UK..

Copeland, R. J.; Alptekin, G.; Cessario, M.; Gerhanovich, Y., 2001. A novel CO_2 separation System. Proceedings of the First National Conference on Carbon Sequestration, , DOE/NETL. Washington, DC. LA-UR-00-1850.

Cho, P., Mattisson, T., Lyngfelt, A., 2004. Comparison of iron-, nickel-, copper- and manganese-based oxygen carriers for chemical-looping combustion. Fuel, 83, 1215-1225.

De Diego, L. F., Gayán, P., García-Labiano, F., Celaya, J., Abad, A., Adánez, J., 2005. Impregnated CuO/Al_2O_3 oxygen carriers for chemical-looping combustion: Avoiding fluidized bed agglomeration. Energy Fuels, 19, 1850-1856.

García-Labiano, F., de Diego, L. F., Adánez, J., Abad, A., Gayán, P., 2004. Reduction and oxidation kinetics of a copper-based oxygen carrier prepared by impregnation for chemical-looping combustion. Industrial Engineering Chemistry Research 43, 8168-8177.

García-Labiano, F., Adánez, J., de Diego, L. F., Gayán, P., Abad, A., 2005. Effect of pressure on the behavior of copper-, iron-, and nickel-based oxygen carriers for chemical-looping combustion. Energy Fuels (Web release date: November 2, 2005)

IPCC special report on carbon dioxide capture and storage. 2005. (available at http://ipcc.ch). Chapter 3. Capture.

Ishida, M., Zheng, D., Akehata, T., 1987. Evaluation of a chemical-looping combustion power-generation system by graphic exergy analysis. Energy, 12, 147-154.

Ishida, M, Jin, H., Okamoto, T., 1996. A fundamental study of a new kind of medium material for chemical-looping combustion. Energy Fuels, 10, 958-963.

Johansson, E., Lyngfelt, A., Mattisson, T., Johnsson, F., 2003. Gas leakage measurements in a cold model of an interconnected fluidized bed for chemical-looping combustion. Powder Technology 134, 210-217.

Kerr, H. R. 2005. Capture and separation technologies gaps and priority research needs. In *Carbon Dioxide Capture for Storage in Deep Geologic Formations - Results from the CO_2 Capture Project*. Thomas, D., Benson, S. Eds.Volume 1, Chapter 38. Elsevier Ltd., Oxford, UK.

Kronberger, B., Johansson, E., Löffler, G., Mattisson, T., Lyngfelt, A., Hofbauer, H., 2004. A two-compartment fluidized bed reactor for CO_2 capture by chemical-looping combustion. Chemical Engineering Technology 27, 1318-1326.

Kronberger, B., Lyngfelt, A., Löffler, G., Hofbauer, H., 2005a. Design and fluid dynamic analysis of a bench-scale combustion system with CO_2 separation - chemical-looping combustion. Industrial Engineering Chemistry Research 44, 546-556.

Kronberger, B., Löffler, G., Hofbauer, H., 2005b. Simulation of mass and energy balances of a chemical-looping combustion system. Clean Air 6, 1-14.

Levenspiel, O. The Chemical Reactor Omnibook. 1986. Ed. Reverté. Barcelona.

Lim, K. S., Zhu, J. X., Grace, J. R., 1995. Hydrodynamics of gas-solid fluidization. International Journal of Muliphase Flow, 21, 141-193.

Lyngfelt, A., Leckner, B., Mattisson, T., 2001. A fluidized-bed combustion process with inherent CO_2 separation. Application of chemical-looping combustion. Chemical Engineering Science, 56, 3101-3113.

Lyngfelt, A., Kronberger, B., Adánez, J., Morin, J.-X., Hurst, P., 2005. The Grace Project. Development of oxygen carrier particles for chemical-looping combustion. Design and operation of a 10 kW chemical-looping combustor. Proceedings of the 7th International Conference of Greenhouse Gas Control Technologies, Rubin, E. S., Keith, D. W., Gilboy, C. F. Eds. Volume I, pp. 115. Elsevier Ltd., Oxford, UK.

Lyngfelt, A., Thunman, H., 2005. Construction and 100 h operational experience of a 10-kW chemical looping combustor. In *Carbon Dioxide Capture for Storage in Deep Geologic Formations - Results from the CO_2 Capture Project*. Thomas, D., Benson, S. Eds. Volume 1, Chapter 36. ElsevierLtd.,Oxford, UK.

Mattisson, T., Lyngfelt, A., 2001. Capture of CO_2 using chemical-looping combustion; Scandinavian-Nordic Section of Combustion Institute: Göteborg, Sweden.

Mattisson, T., Jardnas, A., Lyngfelt, A., 2003. Reactivity of some metal oxides supported on alumina with alternating methane and oxygen-application for chemical-looping combustion. Energy Fuels, 17, 643-651.

Rao, A. B., Rubin, E. S., 2002. A technical, economic and environmental assessment of amine-based CO_2 capture technology for power plant greenhouse gas control. Environmental Science Technology 36, 4467-4475.

Ritcher, H., Knoche, K., 1983. Reversibility of combustion process. ACS Symposium Series 235, 71-85.

Ryu, H.-J., Bae, D.-H., Han, K.-H., Lee, S.-Y., Jin, G.-T., Choi, J.-H., 2001. Oxidation and reduction characteristics of oxygen carrier particles and reaction kinetics by unreacted core model. Korean Journal of Chemical Engineering 18, 831-837.

Ryu, H.-J., Jin, G.-T., Yi, C.-K., 2005. Demonstration of inherent CO_2 separation and no NO_x emission in a 50 kW chemical-looping combustor: Continuous reduction and oxidation experiment. Proceedings of the 7th International Conference of Greenhouse Gas Control Technologies, Wilson, M., Morris, T., Gale, J., Thambimutu, K. Eds. Volume II, pp. 1907. Elsevier Ltd., Oxford, UK.

Smolders, K., Baeyens, J., 2001. Gas fluidized beds operating at high velocities: A critical review of occurring regimes. Powder Technology 119, 269-291.

Takeuchi, H., Hirama, T., Chiba, T., Biswas, J., Leung, L. S., 1986. A quantitative regime diagram for fast fluidization. Powder technology 47, 195-199.

U.S. Gelogical Survey. *Mineral Commodities Suymmaries 2005*; United States Government Printing Office: Washington, DC, 2005 (available at http://minerals.usgs.gov/minerals).

Wolf, J., Anheden, M., Yan, J., 2001. Performance analysis of combined cycles with chemical looping combustion for CO_2 capture. Proceedings of the 18th Annual International Pittsburg Coal Conference, NewCastle, New South Wales, Australia, pp. 1122-1139.

Wolf, J., Anheden, M., Yan, J., 2005. Comparison of nickel- and iron-based oxygen carriers in chemical looping combustion for CO_2 capture in power generation. Fuel 84, 993-1006.

Captions of the Figures.

Fig. 1. Process scheme of Chemical-Looping Combustion system.

Fig. 2. Conversion versus time curves for the reduction and oxidation reactions of the three oxygen carriers used in this work with different fuel gases. C=15 vol %.

Fig. 3. Solid circulation rates for different metal oxides and fuel gases. 1 MW_f. S=0.2 m^2/MW_f. Lines in Y axis: ‾ ‾ ‾ ‾ ‾ , maximum values of G_s considered feasible for operation without extra costs in riser design and commercially proven; minimum values of G_s to fulfil the heat balance asuming a ΔT_{AR-FR}=50 ºC for the NiO-CH_4 (‾ · ‾ · ‾) and Fe_2O_3-CH_4 (‾ · · ‾ · · ‾) systems.

Fig. 4. Effect of the metal oxide content and ΔX_s on the temperature in the fuel reactor for the combustion of CH_4 with Ni-based oxygen carriers. T_{AR} = 950 ºC; inert= Al_2O_3.

Fig. 5. Relation between the metal oxide content of the oxygen carrier and ΔX_s to get a temperature gradient of 50 ºC between the fuel and air reactors. Solid lines=endothermic reactions. Discontinuous lines= exothermic reductions. Syngas composition (SG) = 67% vol CO and 33% vol H_2; T_{FR}=950 ºC for Fe- and Ni-based oxygen carriers; T_{AR}=800 ºC for Cu-based oxygen carriers; inert= Al_2O_3.

Fig. 6. Total solids inventory of Ni40Al-FG oxygen carrier in the fuel and air reactors for the combustion of 1 MW of CH_4. Discountinous line: minimum solids inventory at a fixed ΔX_s.

Fig. 7. Graph to calculate the solids inventory in CLC systems for any oxygen carrier and fuel gas. Solid lines: reactivity guide lines to calculate the minimum solids inventory in the system. Reaction model: shrinking core model under chemical reaction control for spherical grains. An example of the diagram utilisation is given in the text.

Fig. 8. Solids circulation rates and total solids inventory per MW of CH_4 as a function of the variation of the solid conversion between the fuel and air reactors, ΔX_s. Oxygen carriers: ‾ ‾ ‾ ‾ ‾ Cu10Al-I; ——— , Fe45Al-FG, ‾ · ‾ · ‾ , Ni40Al-FG.

Fig. 9. Minimum solids inventories in the CLC system (—————) as a function of reactivity (τ_i) and oxygen transport capacity (R_o) of the oxygen carrier, and its relation with the solids circulation rate (– – – – –). Fuel gas: CH_4. Dots correspond to the values of the oxygen carriers used in this work.

Fig. 10 (a) Cost of oxygen carrier per tonne of CO_2 avoided as a function of the makeup flow of oxygen carrier for different costs of oxygen carrier, C_{OC}. C_{OC}(Cu10Al-I) = 1.7 \$/kg; C_{OC}(Fe45Al-FG)=1.2 \$/kg; C_{OC}(Ni40Al-FG)=7.7 \$/kg. (b) Effect of the makeup flow on the lifetime of the oxygen carriers for different total solids inventories defined per kg/s of CO_2 avoided. Dashed lines: combustion of CH_4 with the oxygen carriers used in this work and considering the minimum solids inventories for ΔX_s=0.3. ($\mu_{OC} = 2350$ (Cu10Al-I), 3100 (Fe45Al-FG), 820 (Ni40Al-FG)). (■, – – – – – Cu10Al-I; ▲, —·—·—·— , Fe45Al-FG; ●, —·—·—·— , Ni40Al-FG).

Figure 1.

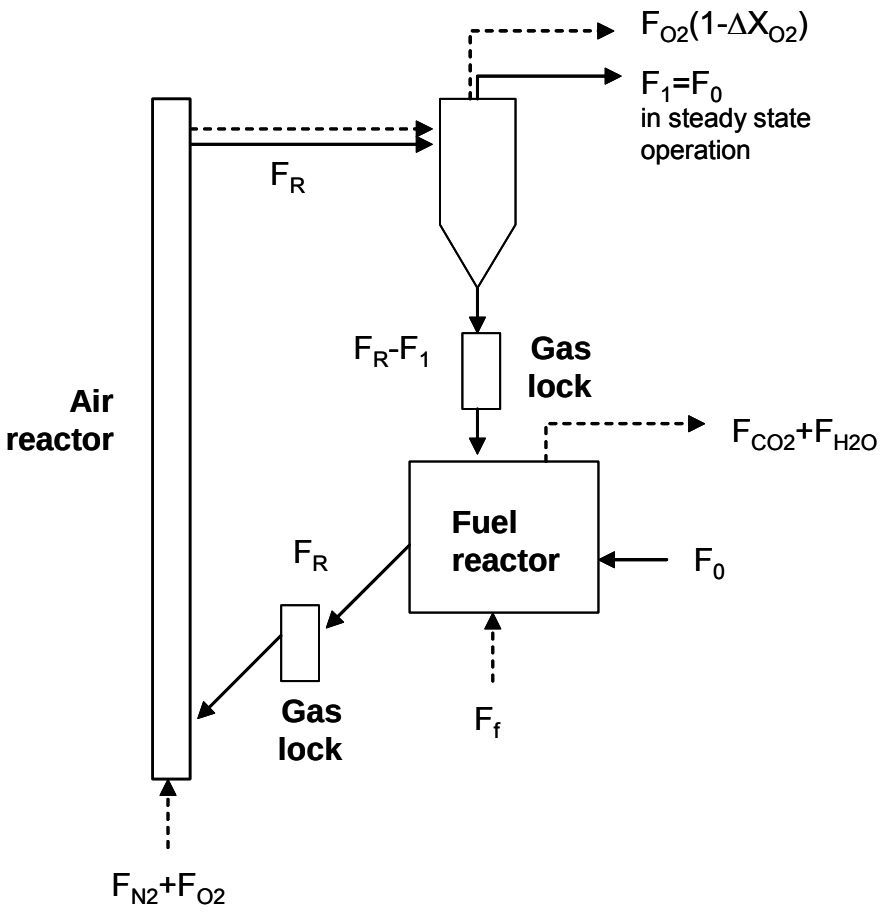
$F_{O2}(1-\Delta X_{O2})$
$F_1=F_0$
in steady state operation
F_R
F_R-F_1
Gas lock
Air reactor
$F_{CO2}+F_{H2O}$
Fuel reactor
F_R
F_0
Gas lock
F_f
$F_{N2}+F_{O2}$

Figure 2.

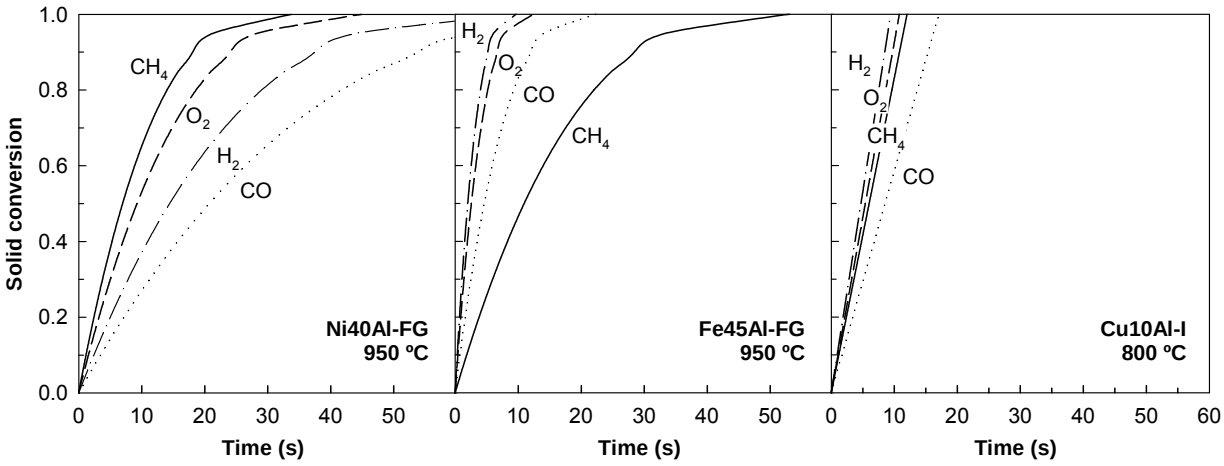
Solid conversion
Time (s)
CH4
O2
H2
CO
Ni40Al-FG
950 ºC
Fe45Al-FG
950 ºC
Cu10Al-I
800 ºC

Figure 3

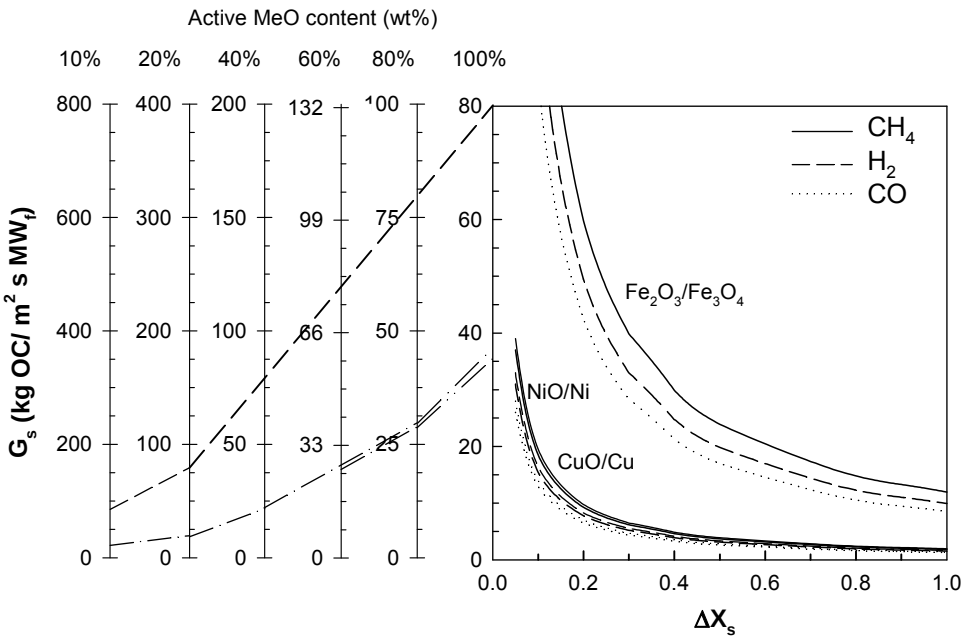
Active MeO content (wt%)
10%
20%
40%
60%
80%
100%
800
600
400
200
0
400
300
200
100
0
200
150
100
50
0
132
99
66
33
0
100
75
50
25
0
80
60
40
20
0
0.0
0.2
0.4
0.6
0.8
1.0
G_s (kg OC/ m^2 s MW_f)
ΔX_s
CH_4
H_2
CO
Fe_2O_3/Fe_3O_4
NiO/Ni
CuO/Cu

Figure 4.

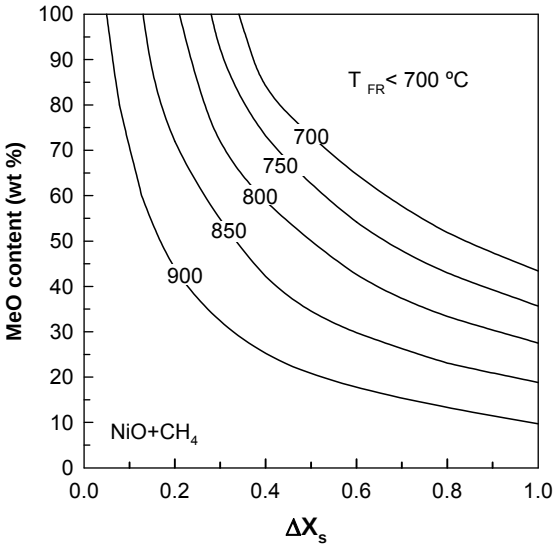
MeO content (wt %)
ΔX_s
T_FR< 700 ºC
700
750
800
850
900
NiO+CH4
0
10
20
30
40
50
60
70
80
90
100
0.0
0.2
0.4
0.6
0.8
1.0

Figure 5.

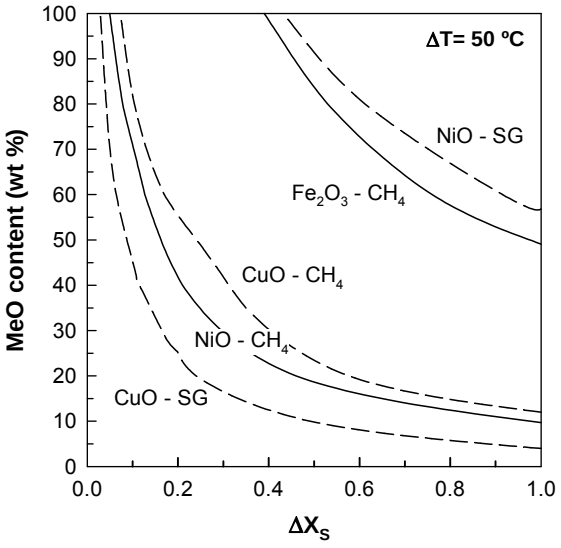
ΔT= 50 ºC
NiO - SG
Fe2O3 - CH4
CuO - CH4
NiO - CH4
CuO - SG
MeO content (wt %)
ΔXS
0
10
20
30
40
50
60
70
80
90
100
0.0
0.2
0.4
0.6
0.8
1.0

Figure 6.

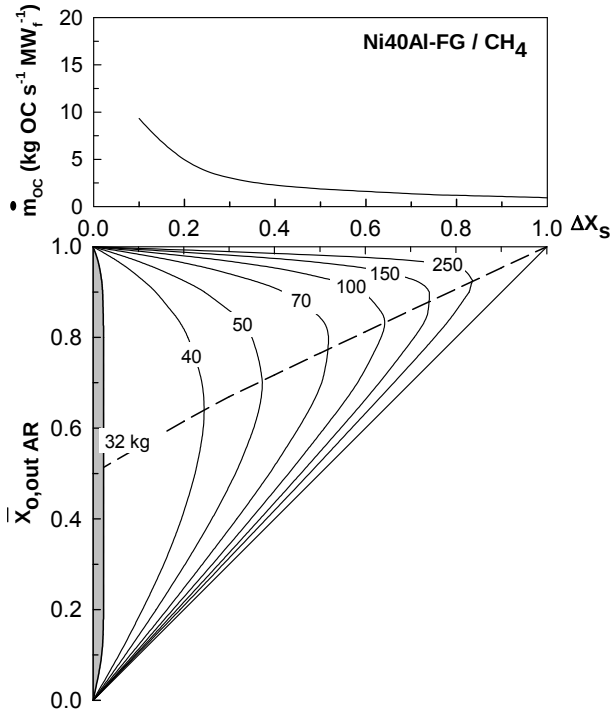
Ni40Al-FG / CH4
ṁoc (kg OC s-1 MWf-1)
20
15
10
5
0
0.0
0.2
0.4
0.6
0.8
1.0
ΔXs
1.0
0.8
0.6
0.4
0.2
0.0
X̄O,out AR
250
150
100
70
50
40
32 kg

Figure 7.

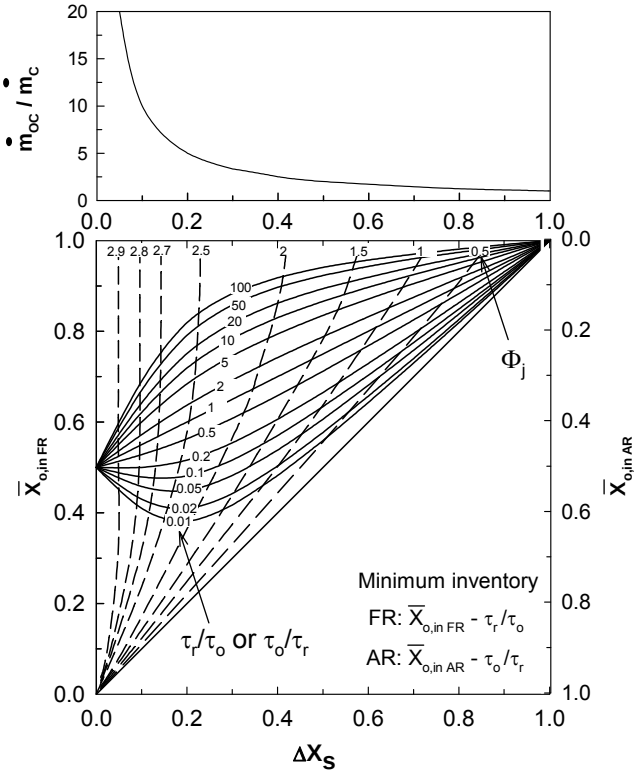
$\dot{m}_{OC} / \dot{m}_c$
$\bar{X}_{o,in\ FR}$
$\bar{X}_{o,in\ AR}$
Δx_S
Φ_j
τ_r/τ_o or τ_o/τ_r
Minimum inventory
FR: $\bar{X}_{o,in\ FR}$ - τ_r/τ_o
AR: $\bar{X}_{o,in\ AR}$ - τ_o/τ_r

Figure 8

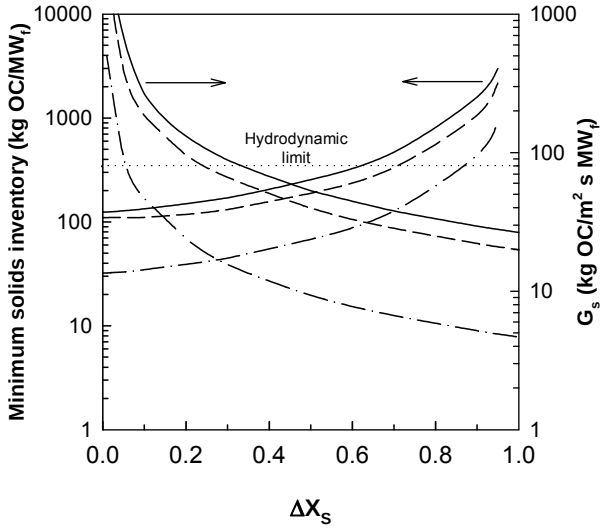
Minimum solids inventory (kg OC/MW$_t$)
G_s (kg OC/m^2 s MW$_t$)
Hydrodynamic limit
10000
1000
100
10
1
1000
100
10
1
0.0
0.2
0.4
0.6
0.8
1.0
ΔX_s

Figure 9

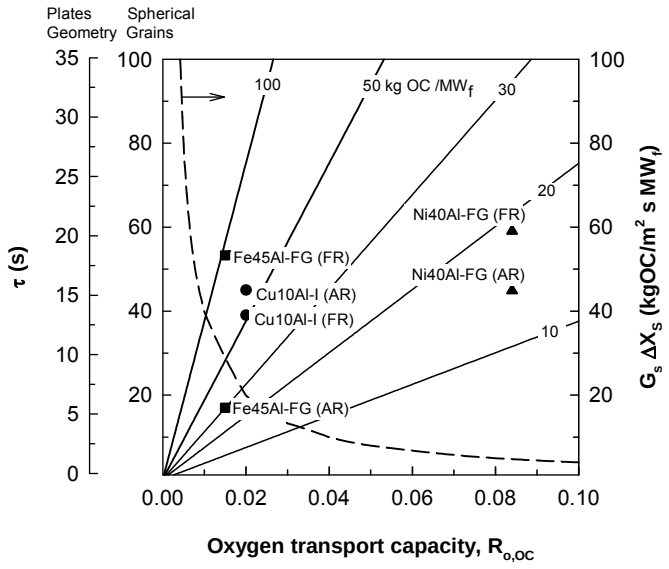
Plates Geometry
Spherical Grains
τ (s)
$G_s \Delta X_s$ (kgOC/m^2 s MW$_f$)
Oxygen transport capacity, $R_{o,OC}$
50 kg OC /MW$_f$
100
30
20
10
Fe45Al-FG (FR)
Cu10Al-I (AR)
Cu10Al-I (FR)
Fe45Al-FG (AR)
Ni40Al-FG (FR)
Ni40Al-FG (AR)

Figure 10

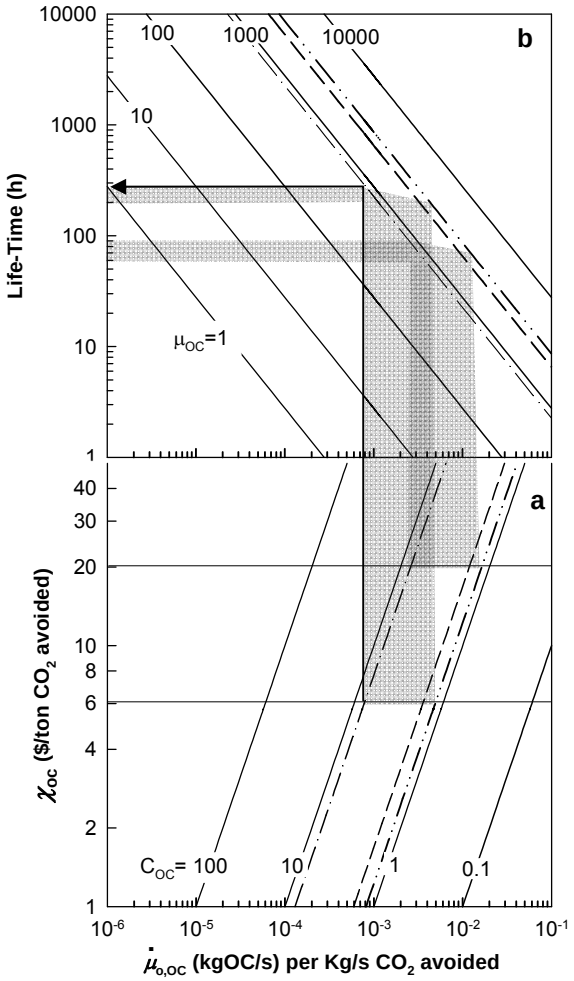
b
a
Life-Time (h)
χ_{oc} ($/ton CO_2 avoided)
$\dot{\mu}_{o,oc}$ (kgOC/s) per Kg/s CO_2 avoided
μ_{OC}=1
C_{OC}= 100
10
1
0.1
100
1000
10000

Table 1. Reactions of the metal oxides used in CLC, oxygen transport capacity of the materials, R_o, and combustion heat at standard conditions (298.15 K, 0.1 MPa).

		R_o	ΔH_c^0 (kJ/mol)
CuO/Cu		0.20	
	$CH_4 + 4\ CuO \longleftrightarrow 4\ Cu + CO_2 + 2\ H_2O$		- 178.0
	$H_2 + CuO \longleftrightarrow Cu + H_2O$		- 85.8
	$CO + CuO \longleftrightarrow Cu + CO$		- 126.9
	$O_2 + 2\ Cu \longleftrightarrow 2\ CuO$		- 312.1
Fe_2O_3 /Fe_3O_4		0.03	
	$CH_4 + 12\ Fe_2O_3 \longleftrightarrow 8\ Fe_3O_4 + CO_2 + 2\ H_2O$		141.6
	$H_2 + 3\ Fe_2O_3 \longleftrightarrow 2\ Fe_3O_4 + H_2O$		- 5.8
	$CO + 3\ Fe_2O_3 \longleftrightarrow 2\ Fe_3O_4 + CO_2$		- 47.0
	$O_2 + 4\ Fe_3O_4 \longleftrightarrow 6\ Fe_2O_3$		- 471.9
NiO/Ni		0.21	
	$CH_4 + 4\ NiO \longleftrightarrow 4\ Ni + CO_2 + 2\ H_2O$		156.5
	$H_2 + NiO \longleftrightarrow Ni + H_2O$		- 2.1
	$CO + NiO \longleftrightarrow Ni + CO_2$		- 43.3
	$O_2 + 2\ Ni \longleftrightarrow 2\ NiO$		- 479.4
Others			
	$CH_4 + 2\ O_2 \longleftrightarrow CO_2 + 2\ H_2O$		- 802.3
	$H_2 + 0.5\ O_2 \longleftrightarrow H_2O$		- 241.8
	$CO + 0.5\ O_2 \longleftrightarrow CO_2$		- 282.9

Table 2. Properties of the oxygen carriers.

	Cu10Al-I	Fe45Al-FG	Ni40Al-FG
Total MeO content (wt %)	13	60	60
Active MeO content (wt %)	10	45	40
Particle size (mm)	0.17	0.15	0.2
Porosity	0.57	0.30	0.36
Specific surface area BET (m^2 g^{-1})	41.3	2.5	0.8
Apparent density (kg m^{-3})	1800	3257	3446
Oxygen transport capacity, $R_{o,OC}$	0.02	0.013	0.084

Table 3. Kinetic parameters of the oxygen carriers.

	Cu10Al-I				Fe45Al-FG				Ni40Al-FG			
	CH4	**H_2**	**CO**	**O_2**	**CH4**	**H_2**	**CO**	**O_2**	**CH4**	**H_2**	**CO**	**O_2**
Physical parameters												
ρ_m (mol/m^3)	**80402**	**80402**	**80402**	**140251**	**32811**	**32811**	**32811**	**22472**	**89290**	**89290**	**89290**	**151520**
r_g or L (m)	**$4.0\ 10^{-10}$**	**$4.0\ 10^{-10}$**	**$4.0\ 10^{-10}$**	**$2.3\ 10^{-10}$**	**$2.6\ 10^{-7}$**	**$2.6\ 10^{-7}$**	**$2.6\ 10^{-7}$**	**$2.6\ 10^{-7}$**	**$6.9\ 10^{-7}$**	**$6.9\ 10^{-7}$**	**$6.9\ 10^{-7}$**	**$5.8\ 10^{-7}$**
b	**4**	**1**	**1**	**2**	**12**	**3**	**3**	**4**	**4**	**1**	**1**	**2**
Kinetic parameters [a]												
k_0 (mol^{1-n} m^{3n-2} s^{-1})	**$4.5\ 10^{-4}$**	**$1.0\ 10^{-4}$**	**$5.9\ 10^{-6}$**	**$4.7\ 10^{-6}$**	**$8.0\ 10^{-3}$**	**$2.3\ 10^{-3}$**	**$6.2\ 10^{-4}$**	**$3.1\ 10^{-4}$**	**$7.1\ 10^{-1}$**	**$9.3\ 10^{-3}$**	**$5.2\ 10^{-3}$**	**$1.8\ 10^{-3}$**
E (kJ/mol)	**60**	**33**	**14**	**15**	**49**	**24**	**20**	**14**	**78**	**26**	**25**	**7**
n	**0.4**	**0.6**	**0.8**	**1.0**	**0.3**	**0.8**	**1.0**	**1.0**	**0.8**	**0.5**	**0.8**	**0.2**
Effect of pressure												
q		**0.53**	**0.83**	**0.68**	**--**	**1.03**	**0.89**	**0.84**	**--**	**0.47**	**0.93**	**0.46**
$\dot{m}_c$ **(kgOC/sMW$_f$)**	**3.97**	**3.28**	**2.81**	**--**	**5.30**	**4.40**	**3.76**	**--**	**0.93**	**0.77**	**0.66**	**--**
$\overline{C}_g$ (vol %)	**13**	**24**	**19**	**11**[b]	**15**	**19**	**14**	**11**[b]	**13**	**24**	**19**	**12**[b]

a. Obtained at atmospheric pressure

b- Considering an air excess of 20 %

Table 4. Solid inventory data per MW of fuel for the different oxygen carriers.

		Cu10Al-I			Fe45Al-FG			Ni40Al-FG		
	Pressure	CH_4	H_2	CO	CH_4	H_2	CO	CH_4	H_2	CO
Minimum solids inventory										
$m_{OC,FR}$ (Kg OC)	1	52	23	45	94	12	29	18	13	19
$m_{OC,AR}$ (Kg OC)	1	60	49	42	30	25	21	14	12	10
Minimum solids inventory at Δx=0.3										
$m_{OC,FR}$ (Kg OC)	1	62	29	54	126	17	40	25	18	25
$m_{OC,AR}$ (Kg OC)	1	71	57	50	44	34	30	20	16	14
Minimum solids inventory at Δx=0.3[a]										
$m_{OC,FR}$ (Kg OC)	10	--	25	58	--	29	31	--	17	34
$m_{OC,AR}$ (Kg OC)	10	34	27	24	30	24	21	32	26	23

a. Values calculated assuming a decrease of solids reactivity with increasing total pressure according to Eq. (5).